Name of Journal: *Géotechnique*

Paper Type: Research Paper

Date of Submission: 27 January 2021

Coupling cyclic and water retention response of a clayey sand subjected to traffic and environmental cycles

Arash Azizi[1], Ashutosh Kumar[2] and David G. Toll[3*]

[1] Research Fellow, Department of Engineering, Durham University, United Kingdom. email: arash.azizi@durham.ac.uk

[2] Assistant Professor, School of Engineering, IIT Mandi, India. Formerly Postdoctoral Research Associate, Department of Engineering, Durham University, United Kingdom. email: ashutosh@iitmandi.ac.in

[3] Professor, Department of Engineering, Durham University, United Kingdom. email: d.g.toll@durham.ac.uk

* Corresponding author

Number of words: 8504

Number of figures: 16

Number of tables: 4

ABSTRACT

Compacted soils used as formation layers of railways and roads continuously undergo water content and suction changes due to seasonal variations. Such variations together with the impact of cyclic traffic-induced loads can alter the hydro-mechanical behaviour of the soil, which in turn affects the performance of the superstructure. This study investigates the impact of hydraulic cycles on the coupled water retention and cyclic response of a compacted soil. Suction-monitored cyclic triaxial tests were performed on a compacted clayey sand. The cyclic response of the soil obtained after applying drying and wetting paths was different to that obtained immediately after compaction. The results showed that both suction and degree of saturation are required to interpret the cyclic behaviour. A new approach was developed using (i) a hysteretic water retention model to predict suction variations during cyclic loading and (ii) Bishop's stress together with a bonding parameter to predict accumulated permanent strain and resilient modulus. The proposed formulations were able to predict the water retention behaviour, accumulated permanent strains and resilient modulus well, indicating the potential capability of using the fundamentals of unsaturated soils for predicting the effects of drying and wetting cycles on the coupled soil water retention and cyclic response.

KEYWORDS: Unsaturated soil; suction; cyclic loading; resilient modulus.

INTRODUCTION

Formation layers of roads and railways are often compacted and exist in an unsaturated condition. These layers continuously undergo cycles of drying and wetting due to environmental loads, which together with repeated traffic loads can affect the cyclic response of soils and lead to premature loss of serviceability of the superstructure (Brown, 1996; Li & Selig, 1998; McCartney & Khosravi, 2013; Stirling et al., 2020). With continuously changing climatic conditions, the coupled effects of cyclic traffic-induced and environmental loads on the cyclic behaviour of formation materials need to be assessed to develop a strategy to mitigate climate-risks at the design stage of road and railway provision.

Experimental results have shown that an increase in water content can increase the accumulated permanent deformation and decrease the resilient modulus of soils under cyclic loading (e.g. Seed et al., 1962; Drumm et al., 1997; Lekarp et al., 2000; Khoury et al., 2009; Cao et al., 2017). It has also been suggested that the soil cyclic response is better correlated with suction rather than water content (e.g. Fredlund et al., 1977; Yang et al., 2008; Ng et al., 2013; Salour & Erlingsson, 2015; Chen et al., 2018). However, many experimental results have revealed that a comprehensive understanding of the behaviour of unsaturated soils requires information on both suction and water saturation (e.g. Toll, 1990; Wheeler et al., 1996; Toll & Ong, 2003; Sivakumar et al., 2013). The hysteretic response of soil suction to drying and wetting cycles results in varied water retention properties (the relationship between suction and water stored in soil pores), which in turn affects the cyclic behaviour of unsaturated soils (e.g. Khalili et al., 2008; Khoury et al., 2011; Ng et al., 2013). Nevertheless, the effects of the hydraulic cycles on the coupled water retention and cyclic behaviour of soils have not been fully addressed, mainly owing to the lack of appropriate experimental data or the absence of a proper coupling approach.

Most studies have employed net stress (the difference between the total stress and air pressure) and suction as independent stress variables to evaluate the accumulated permanent deformation and resilient modulus (e.g. Oloo & Fredlund, 1998; Gupta et al., 2007; Ng et al., 2013; Han et al., 2015). These two stress variables are easy to control under laboratory conditions but provide no information on soil water saturation. In recent years, alternative stress variables have been proposed incorporating water retention properties into the shearing or bulk stress to predict the soil cyclic behaviour (e.g. Heath et al., 2004; Oh et al., 2012; Han & Vanapalli, 2016). Bishop′s stress (Bishop, 1959) has been a well-known stress choice to account for the impact of suction (s) and degree of saturation (S_r) on the soil cyclic response (Liang et al. 2008; Zhou & Ng, 2016; Blackmore et al., 2020). Bishop′s stress $\boldsymbol{\sigma}^*$ is defined as:

$$\boldsymbol{\sigma}^* = \boldsymbol{\sigma}_n + \chi s\boldsymbol{I} \quad (1)$$

where $\boldsymbol{\sigma}_n$ is net stress, χ has been commonly assumed to be equal to degree of saturation and $\boldsymbol{I}$ is the identity tensor. Jommi (2000) explained that Bishop′s stress accounts for the effect of suction on the average stress acting on the soil skeleton. However, suction also influences the normal force acting at soil particle contacts due to the presence of water menisci (Wheeler et al., 2003). Gallipoli et al. (2003) then proposed a bonding parameter ξ as an additional constitutive variable to consider the latter effect (called "suction bonding" in this paper):

$$\xi = (1 - S_r)f_s \quad (2)$$

where $(1 - S_r)$ accounts for the number of water menisci per unit soil volume and f_s accounts for the increase in the inter-granular force exerted by a single meniscus with suction. The bonding parameter, in addition to the skeleton stress, has been used to reproduce various mechanical features of unsaturated soils under monotonic loading conditions (e.g. Gallipoli et al., 2003; Tarantino & Tombolato, 2005; Tarantino, 2007; Hu et al., 2015), but its application to the cyclic behaviour has not been explored. To the authors' knowledge, only Ng & Zhou (2014) and Zhou & Ng (2016) used these two variables to explain the effect of temperature on the cyclic response of a clayey soil.

This research examined the water retention properties of a clayey sand after compaction and after applying drying and wetting paths. Also, the cyclic behaviour of the compacted soil before and after applying hydraulic loads were studied using a suction-monitored cyclic triaxial system. The coupling effects of soil water retention and cyclic response were then addressed by: (i) tackling the impact of accumulated strains and degree of saturation on the measured suction using a hysteretic water retention model (ii) accounting for the impact of the soil water retention properties on the accumulated permanent strains and resilient modulus using two constitutive variables: Bishop′s stress and the bonding parameter. Semi-empirical models were proposed incorporating the effects of the hydraulic history on the observed water retention behaviour, accumulated permanent strains and resilient modulus providing insights into the coupled hydro-mechanical behaviour of a formation material subjected to cyclic traffic and environmental loads.

MATERIAL AND SAMPLE PREPARATION

The tested soil was taken from a railway line constructed along the southeastern coast of South Africa to transport coal from around 40 mines to Richards Bay Coal Terminal. The formation layers of the railway embankment comprise 40 cm of fill material below the ballast and sub-ballast layers. This study presents results of the tests performed on the fill material (named as "CLASS B" e.g. in Gräbe & Clayton, 2009), in this case a clayey sand containing 79% sand, 12% silt and 9% clay. The liquid limit LL and plastic index PI of the fines are 25% and 9%, respectively, and the specific gravity G_s is 2.66 (BS 1377-2, 1990).

Compaction

The oven-dried soil was mechanically ground, then the soil powder was mixed with a controlled amount of water and kept in a sealed bag at least 24 hours to allow water content equilibration. Next, the soil was placed in a Proctor mould and dynamically compacted using 25 blows of the 2.5 kg standard Proctor hammer (BS 1377-4, 1990) in four layers. A steel sharp tube was intruded into the compacted specimen and a smaller specimen having a height of 140 mm and a diameter of 70 mm was then extruded from the tube. The water content w was measured to be 10.7±0.07% and dry density ρ_d to be 1.820±0.015 Mg/m^3 (96 - 98% compaction considering the maximum dry density of 1.871 Mg/m^3 obtained from the standard proctor compaction curve), i.e. just wet of optimum w = 10.2% (this is consistent with the values reported by Blackmore et al., 2020). The specimens were compacted slightly on the wet side to ensure initial suctions were within the measurement range of the tensiometer. This also allowed studying the effect of intense drying while the specimens underwent a larger suction variation during first drying. Moreover, the compacted soil fabric was more uniform (less aggregated) on the wet side compared to the case of optimum or on the dry side.

Drying and wetting

3 specimens were tested after compaction (named "As", to indicate as-compacted) whereas the other 14 specimens were subjected to different drying and wetting paths before cyclic triaxial testing to mimic the effect of environmental loads on the in-situ material. The drying path was imposed by air-drying at a constant temperature of 20°C (±0.5°C) and relative humidity of 34% (15 – 90 hours depending on the target water content level). The wetting path was imposed by placing the specimen in a closed chamber at a high relative humidity close to 100% (20 – 25 days depending on the target water content level). The rate of evaporation during drying and water intake during wetting was the same for all the specimens so different water content levels imply that the specimens were

dried out or wetted up for different time periods. The weight (using a digital balance) and dimensions (using a digital calliper) of the specimen, and hence the water content and density, were measured at average time intervals of 4 hours. The specimens were relatively dense so no disturbance was observed during this process. The volumetric strains measured during drying and wetting were found to be in the range of ±1.25%.

At the end of each hydraulic path, the specimens were wrapped and sealed in a plastic bag for at least 24 hours for water equalisation. The specimens were then mounted on the triaxial pedestal while the suction of the specimens was monitored using a suction probe under constant water content conditions (see detail in the section of Testing Methodology). It was assumed that the water equilibrium was achieved when a constant suction value was measured.

Figure 1 shows the hydraulic paths applied and the ranges of the water content obtained. "1D" indicates the specimens being dried to different water contents along the first drying path, "1W" shows the specimens on the first wetting up (after the first drying path), "2D" indicates the specimen subjected to the second drying path (following the first drying-wetting cycle), "2W" indicates the specimen subjected to 2 cycles of drying and wetting, and similarly "3W" indicates specimens subjected to 3 cycles of drying and wetting. It is to be noted that drying was continued to a fully air-dried state (the suction at the fully air-dried condition was 146.1 MPa) before applying the wetting path. Table 1 shows the properties of the as-compacted specimens (As) and those subjected to drying and wetting after compaction (1D, 1W, 2D, 2W and 3W).

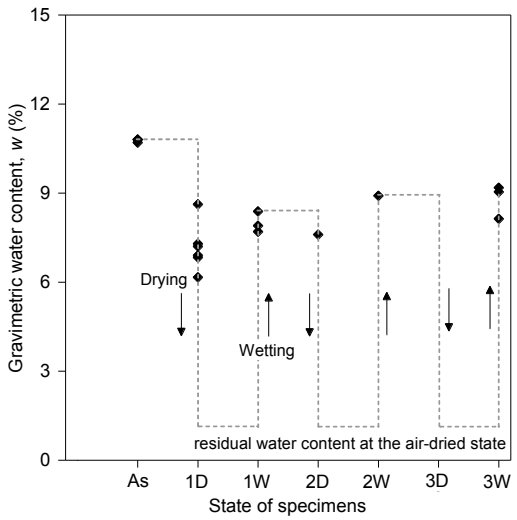

Fig 1. Water content of the specimens after compaction and after hydraulic loading

Table 1. Details of triaxial specimens after preparation

Title	ρ_d (Mg/m^3)	w (%)	s (kPa)	S_r (%)	Specimen state
As1q40*	1.838	10.80	40	64.29	As-compacted
1D1q40	1.882	8.62	140	55.51	1st drying
1D2q40	1.880	7.21	420	46.21	1st drying
1D3q40*	1.841	7.29	259	43.57	1st drying
2D1q40	1.871	7.60	104	47.97	2nd drying
1W1q40*	1.815	8.38	39	47.86	1st wetting
2W1q40	1.880	8.91	33	57.11	2nd wetting
3W1q40	1.812	8.13	60	46.24	3rd wetting
3W2q40	1.837	9.04	34	53.66	3rd wetting
As1q60	1.833	10.80	40	63.73	As-compacted
1D1q60	1.860	6.91	390	42.69	1st drying
1W1q60	1.872	7.89	70	49.90	1st wetting
As1q80	1.813	10.70	45	60.94	As-compacted
1D1q80	1.874	6.16	511	39.09	1st drying
1D2q80	1.840	6.82	220	40.70	1st drying
1W1q80	1.870	7.70	50	48.51	1st wetting
3W1q80	1.810	9.18	35	52.04	3rd wetting

* The first number refers to the number of hydraulic cycles; 'As' refers to as-compacted; 'D' refers to the dried specimen; 'W' refers to the wetted specimen; the second number refers to the number of tests under a similar loading condition; 'q' refers to cyclic deviatoric stress and the third number refers to its value, e.g. 'q40' means q_{cyc} = 40 kPa.

Water retention properties

The water retention behaviour of the tested soil compacted at ρ_d = 1.854 Mg/m^3 and w = 12.1% is described in Kumar et al. (2021). Figure 2a shows the water retention curves (WRCs), either continuous (measured by a tensiometer) or discrete (measured by a tensiometer or WP4 Dewpoint Potentiameter), in terms of suction and degree of saturation (please see details of the water retention tests in Kumar et al., 2021). Although WP4 measures the total suction, i.e. matric suction plus osmotic suction, the data from WP4 measurements was combined with the data from the tensiometer measurements, i.e. matric suction. The two sets of data matched well implying that

the osmotic suction was not significant (see a similar approach used in e.g. Romero et al. 2011; Tripathy et al. 2014; Ng et al. 2016).

The hysteretic nature of the water retention behaviour along the drying and wetting paths and the scanning domain bounded by the main WRCs (shown by the dashed lines) can be observed. The continuous drying curve followed a scanning curve until the suction reached about 200 kPa where it met the main drying curve. The continuous wetting curve followed a scanning curve from the suction value of 630 kPa and approached the main wetting curve at the suction value of 10 kPa.

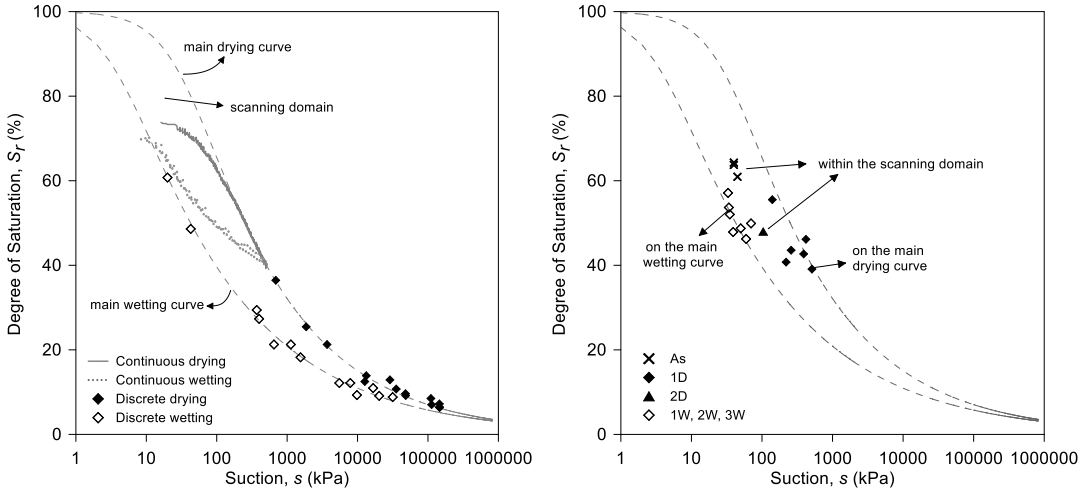

(a) (b)

Fig. 2. a) experimental data of main and scanning WRCs redrawn from Kumar et al. (2021) b) water retention properties of the specimens, prepared for cyclic triaxial testing, after compaction and after applying drying and wetting paths

Figure 2b shows the measured water retention properties of the specimens, prepared for cyclic triaxial testing in this study, after compaction and after applying drying and wetting paths. The average suction of the as-compacted specimens was about 40 kPa and the average degree of saturation was 63.0% implying that their water retention states were within the scanning domain as shown in Figure 2b. The water retention states of the dried specimens lay within the scanning domain or on the main curve depending on the degree of saturation achieved at the end of drying. As all the wetted specimens (1W, 2W and 3W) were wetted up from the air-dried condition (s = 146.1 MPa), their suction and saturation levels lay on the main wetting curve regardless of the number of drying and wetting cycles. The degree of saturation markedly increased along the main wetting curve at s < 100 kPa even

when the decrease in suction was small. Therefore, the wetted specimens had a similar range of suction but different saturation levels. The suction obtained for 2D was lower than 1D at a similar saturation level. This can be explained considering the hydraulic history of 2D where the 2nd drying path was applied from the wet state on the main wetting curve having a lower suction and degree of saturation compared to the as-compacted state that 1D was dried from.

TESTING METHODOLOGY

Cyclic tests were carried out using a triaxial apparatus with on-specimen instrumentation and continuous measurements of volume changes and suction. The volume changes were measured using three mini Linear Variable Differential Transformers (LVDTs), two of them were mounted vertically (with the ability to measure ±2.5 mm) on opposite sides of the specimen for measurement of axial deformations and the other one was mounted horizontally in a radial-strain calliper attached to the mid-height of the specimen for measurement of radial deformations. Direct measurement of suction was achieved using a high capacity tensiometer capable of measuring pore water pressure in the range of ±2MPa (Lourenço et al., 2008; Toll et al. 2013). An access hole was made through the latex membrane covering the specimen, very close to the mid-height, where intimate contact between the tensiometer and soil was achieved by inserting the tensiometer through a rubber grommet. Silica gel was used to coat all around the access hole to ensure no water exchange could take place between the specimen and triaxial cell. During triaxial tests, the air pressure was at atmospheric pressure while the water pressure was negative in the unsaturated specimens; therefore, suction is the measured negative pore water pressure (expressed as a positive value of suction). The fast response of the tensiometer and also the measurement at the specimen mid-height, where the maximum deformation takes place during cyclic loading, allowed monitoring the evolving suction during cyclic testing. The details of the on-specimen instrumentations are described in Kumar et al. (2021). Triaxial tests included isotropic compression followed by stress-controlled cyclic loading under a constant water content condition while the water drainage lines were closed. The water contents of the specimens measured after compaction or at the end of the drying - wetting process (w_i) was very similar to that measured at the end of the cyclic triaxial tests ($w_i \pm 0.1\%$) ensuring that the constant water content condition was satisfied. All specimens were subjected to a confining stress σ_c of 20 kPa (the total stress was equal to the net stress as the air pressure was at atmospheric pressure) typical of the stress considered for a railway embankment (Liu and Xiao, 2010). After isotropic compression, cyclic deviatoric stresses q_{cyc} of 40, 60 and 80 kPa were applied accounting for the stress level at the formation layer typical of empty to fully loaded wagons, while a resting stress of 10 kPa and σ_c of

20 kPa were maintained. The resting stress of 10 kPa ensured a continuous contact between the top of the soil specimen and the loading ram. The sinusoidal deviatoric stress applied is shown in Figure 3a (in this case q_{cyc} = 40 kPa). Specimens were subjected to 1000 load cycles at a frequency of 1Hz which were found to be sufficient cycles to achieve a resilient state.

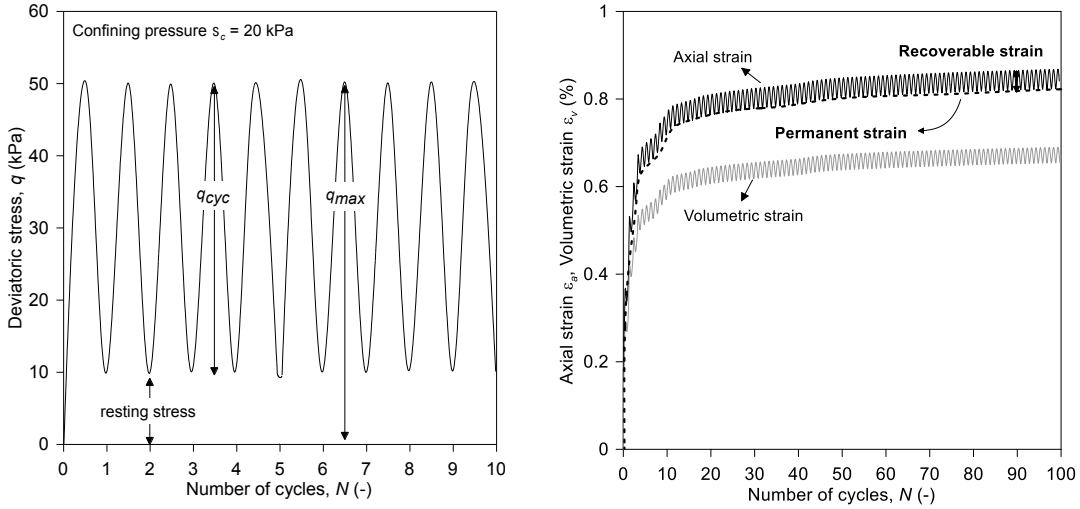

(a) (b)

Fig. 3. Loading and measured strains during cyclic testing a) sinusoidal deviatoric stress pattern b) example of axial and volumetric strain responses

Figure 3b shows the axial and volumetric strains measured for one of the tested specimens during the first 100 cycles. The measured plastic axial deformation was used to define the accumulated permanent strain ε_p and the recoverable axial strain ε_r was used to obtain the resilient modulus M_R (Seed et al., 1962):

$$M_R = \frac{q_{cyc}}{\varepsilon_r} \quad (3)$$

The volumetric strains governed the changes in the degree of saturation during testing under the constant water content condition. The soil exhibited contractive behaviour (positive values of strains) under the given loading conditions.

For cyclic triaxial testing, one of the dried specimens (1D2q80) was repetitively subjected to packets of cyclic loads and wetting to reproduce the field condition of the formation layer periodically subjected to traffic loads and precipitation. During the wetting stages, water was injected through the top of the specimen at a low

infiltration rate (~ 1 g/h). The drainage was open for this test and the water content was obtained from back calculation based on the water content of the specimen measured at the end of the test and the amount of water injected at each wetting stage. The testing approach used was more representative of the natural mechanism of water content variations within soil embankments compared to suction-controlled techniques such as axis translation where cavitation is prevented from occurring within the soil (Toll et al. 2013).

EXPERIMENTAL RESULTS OF CYCLIC TRIAXIAL TESTING

After the specimens were assembled in the triaxial apparatus, a confining pressure σ_c of 20 kPa was applied. The measured volumetric compression of the specimens was less than 1.1%. As a result of compression, the degree of saturation slightly increased leading to a reduction in the suction level. After equilibrium was achieved at the end of the compression stage, the specimens were subjected to cyclic loads. The properties of the specimens obtained after compression and after cyclic loading are presented in Table 2.

Figure 4 shows the cyclic response of As1q40, 1D1q40, 1W1q40 and 2W1q40 (in these cases, q_{cyc} = 40 kPa, with starting states as-compacted, after 1st drying, after the 1st wetting and after 2nd wetting, respectively). The results are presented in terms of the axial strain, suction, degree of saturation and resilient modulus with respect to the number of loading cycles. All the measured variables reached a steady state as the number of cycles approached 1000. Figure 4a shows the axial strain ε_a rapidly increased with the first cycles and then accumulated at a decreasing rate with increasing loading cycles. ε_a decreased from As1q40 (with permanent axial strain ε_p of 1.46%) to 1D1q40 (ε_p = 0.84%) as the suction level increased from 22 kPa to 122 kPa (Figure 4b). ε_p of 1W1q40 and 2W1q40, although having a similar range of suction to As1q40 (~ 29 kPa), showed significantly different strain responses. ε_p of 1W1q40 was measured (ε_p = 0.82%) to be close to ε_p of 1D1q40. However, ε_p of 2W1q40 was found (ε_p = 1.36%) to be higher than that of 1W1q40 and close to ε_p of As1q40.

266 Table 2. Details of triaxial specimens after compression and after cyclic loading

267

Title	After compression			After cyclic loading						Testing condition
	ρ_d (Mg/m^3)	s (kPa)	S_r (%)	q_{cyc} (kPa)	w (%)	s (kPa)	S_r (%)	p^* (kPa)	ξ (-)	
As1q40	1.848	22	65.37	40	10.80	17	67.56	48.5	0.32	Constant water content
1D1q40	1.897	122	57.00	40	8.62	90	58.18	89.0	0.46	Cons. w
1D2q40	1.891	413	47.12	40	7.21	378	47.85	217.6	0.62	Cons. w
1D3q40	1.844	217	43.78	40	7.29	201	44.27	125.7	0.64	Cons. w
2D1q40	1.893	86	49.85	40	7.60	72	50.72	73.2	0.53	Cons. w
1W1q40	1.818	30	48.17	40	8.38	25	49.09	48.9	0.52	Cons. w
2W1q40	1.889	29	58.12	40	8.91	22	59.91	49.8	0.40	Cons. w
3W1q40	1.821	45	46.93	40	8.13	40	47.70	55.7	0.55	Cons. w
3W2q40	1.850	25	54.89	40	9.04	23	56.28	49.3	0.44	Cons. w
As1q60	1.855	22	66.20	60	10.80	20	68.69	57.1	0.31	Cons. w
1D1q60	1.866	360	43.12	60	6.91	320	43.92	183.9	0.66	Cons. w
1W1q60	1.894	60	51.95	60	7.89	40	53.05	64.6	0.49	Cons. w
As1q80	1.821	26	61.75	80	10.70	25	64.48	65.9	0.36	Cons. w
1D1q80	1.876	490	39.20	80	6.16	433	39.87	222.6	0.73	Cons. w
1D2q80	1.860	201	42.15	80	6.82	172	43.15	124.3	0.65	Repetitive loading-wetting
1W1q80	1.892	39	50.49	80	7.70	31	51.73	65.5	0.50	Cons. w
3W1q80	1.829	25	53.76	80	9.18	20	55.56	61.1	0.45	Cons. w

268

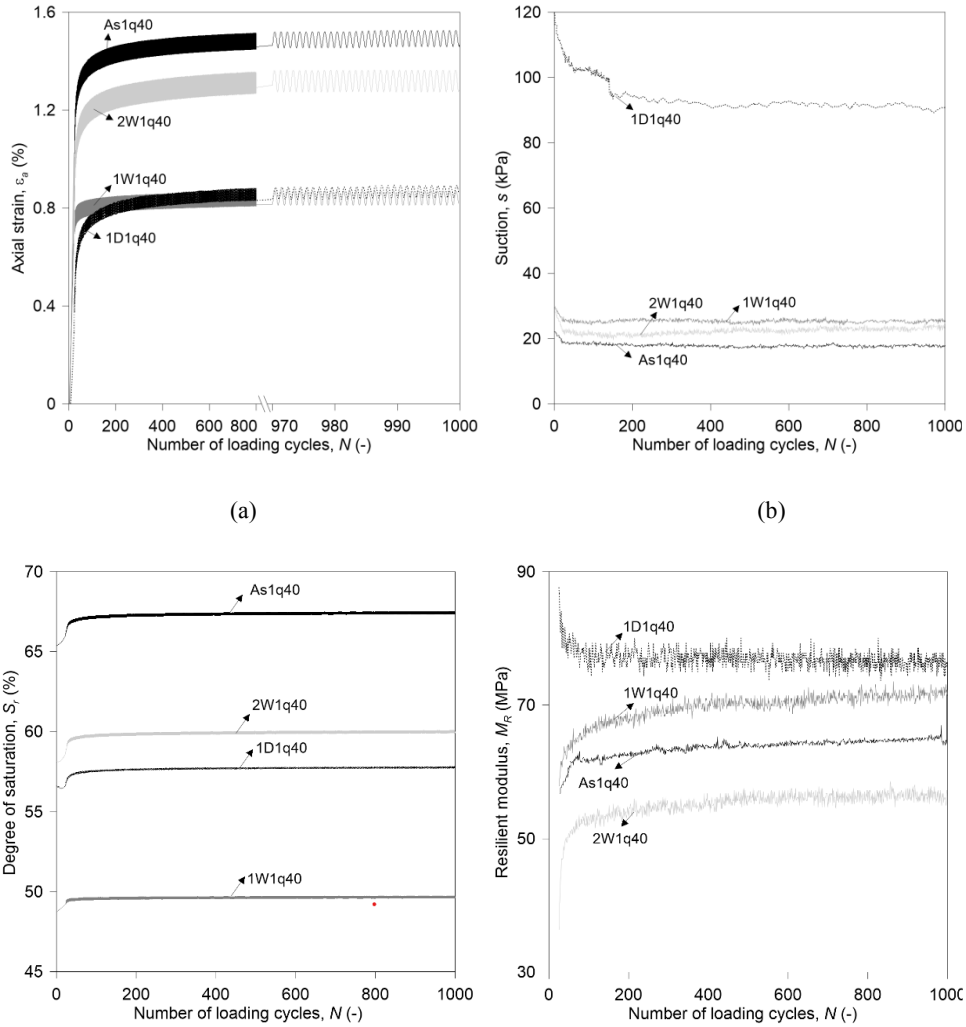

Fig. 4. Cyclic behaviour of As1q40, 1D1q40, 1W1q40 and 2W1q40 with the number of load cycles: a) axial strain, ε_a b) suction, s c) degree of saturation, S_r d) resilient modulus, M_R

The measured suctions decreased during cyclic loading (as also observed by Yang et al., 2008 and Craciun & Lo, 2010) which can be explained by an increase in the degree of saturation S_r (Figure 4c) due to the accumulation of the permanent strains under constant water conditions. S_r of these 4 specimens was different with As1q40 being the highest (S_r = 65.4%). The difference in S_r for the wetted specimens was about 10% (1W1q40 having a value of 48.2% and 2W1q40 with a value of 58.1%). For specimens at the same suction level, the higher the increase in S_r the greater the reduction in suction. The suction variation of 1D1q40 with a higher suction level than the other 3 specimens was evidently greater although the increase in its degree of saturation was smaller. This implies that

279 the variations of suction induced by cyclic loading were not only dependent on the changes in the degree of
280 saturation but also on the suction level.
281 Figure 4d shows that the resilient modulus M_R of As1q40, 1W1q40 and 2W1q40 increased with the number of
282 cycles due to accumulations of permanent strains and progressive densification (as also reported by Sivakumar et
283 al., 2013). On the contrary, M_R of 1D1q40 slightly decreased with the number of cycles owing to the greater
284 reduction in its suction compared to the other 3 specimens. M_R was observed to be higher for 1D1q40 (M_R = 74.7
285 MPa) compared to the other 3 specimens as the suction was higher. M_R of As1q40 was higher than 2W1q40 but
286 lower than 1W1q40 although their suction levels were not very different.
287 The results presented above imply that suction alone cannot exclusively describe the cyclic response of the tested
288 soil being subjected to different hydraulic paths and information on the water saturation level is also required.
289 Figure 5 shows the effect of increasing the cyclic deviator stress from 40kPa (As1q40 and 1D2q40) to 80kPa
290 (As1q80 and 1D1q80). Figure 5a shows that ε_a measured was significantly lower for 1D2q40 and 1D1q80
291 compared to As1q40 and As1q80 as the former cases had higher suction values (Figure 5b) due to being dried
292 after compaction. ε_a was also found to increase with q_{cyc} comparing the accumulated permanent strain ε_p of the
293 specimens having similar suction levels, i.e. As1q40 (ε_p = 1.46%) to As1q80 (ε_p = 1.83%) and 1D2q40 (ε_p =
294 0.47%) to 1D1q80 (ε_p = 0.61%). This increase in the axial strain was greater in the case of the as-compacted
295 specimens where the suction level was low (s < 40 kPa). Figure 5b shows that the decrease in suction for 1D2q40
296 and 1D1q80 was more evident where suction was above 350 kPa. The decrease in suction was slightly larger with
297 the increased q_{cyc} as the increase in the accumulated permanent strain resulted in a greater increase in the degree
298 of saturation as shown in Figure 5c.
299 Figure 5d shows the resilient modulus M_R of 1D2q40 and 1D1q80 decreased with the number of loading cycles
300 which can be explained by the decrease in suction. M_R of As1q40 and As1q80 increased where suction variations
301 were small. This was due to the dominant effect of progressive densification and the resulting increase in S_r. M_R
302 also increased with suction, comparing M_R of the as-compacted to dried specimens, but decreased with the cyclic
303 deviatoric stress. The decrease in the resilient modulus with q_{cyc} was more evident at high suction levels (s > 350
304 kPa) comparing M_R of 1D2q40 (M_R = 161.3 MPa) to 1D1q80 (M_R = 85.7 MPa). This is consistent with the results
305 reported by Thom et al. (2008) and Ng et al. (2013).
306

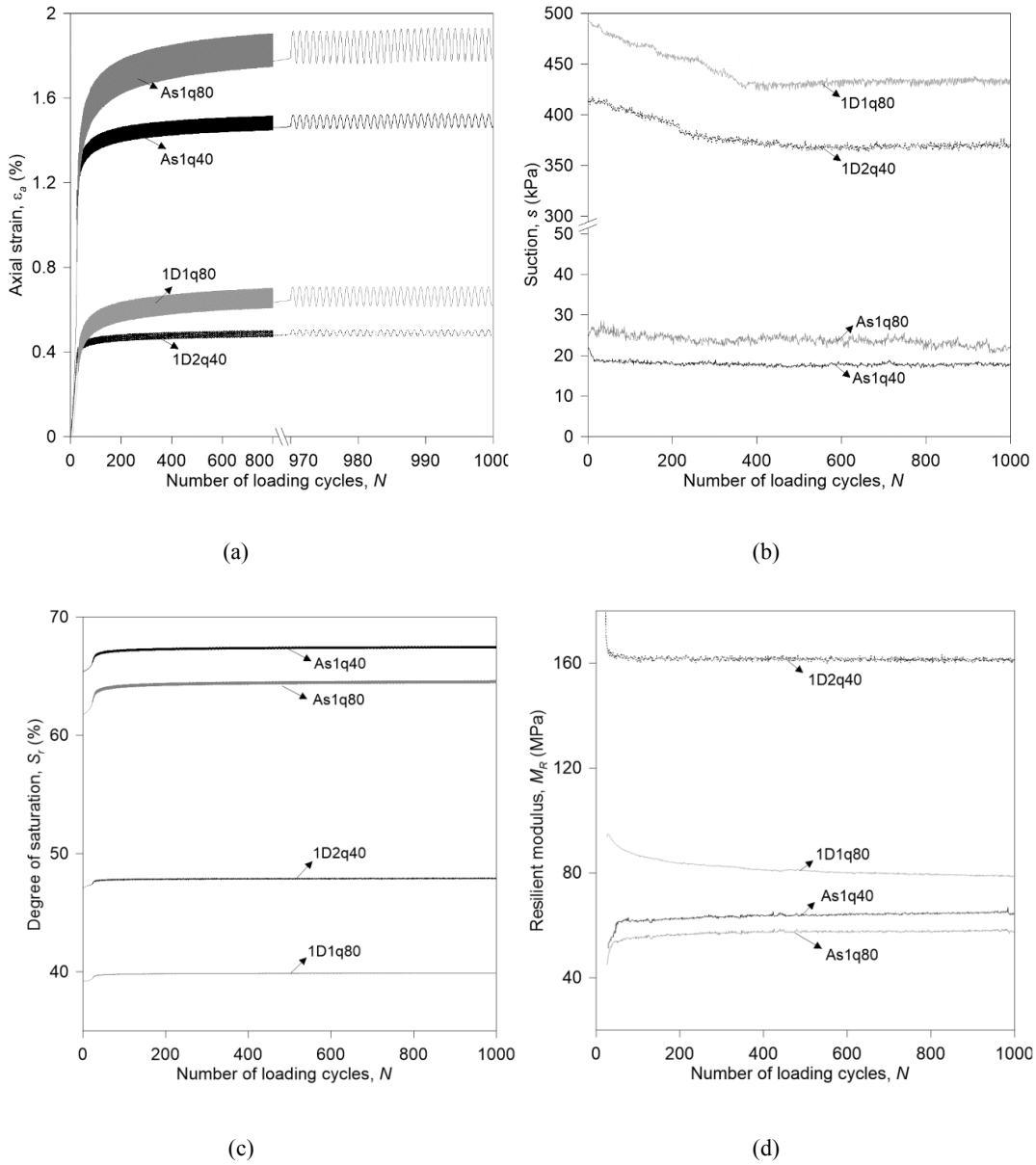

307 Fig. 5. Cyclic behaviour of As1q40, 1D2q40, As1q80 and 1D1q80 with the number of load cycles: a) axial strain,
308 ε_a b) suction, s c) degree of saturation, S_r d) resilient modulus, M_R
309
310 The results show that the accumulated permanent strain increased and M_R decreased with the increase in q_{cyc},
311 implying that the soil resilience decayed with an increase in the cyclic load level. The effect of q_{cyc} on the
312 accumulated permanent strain was found to be more pronounced at low suctions but the equivalent effect on the
313 resilient modulus was more evident at high suction levels.
314

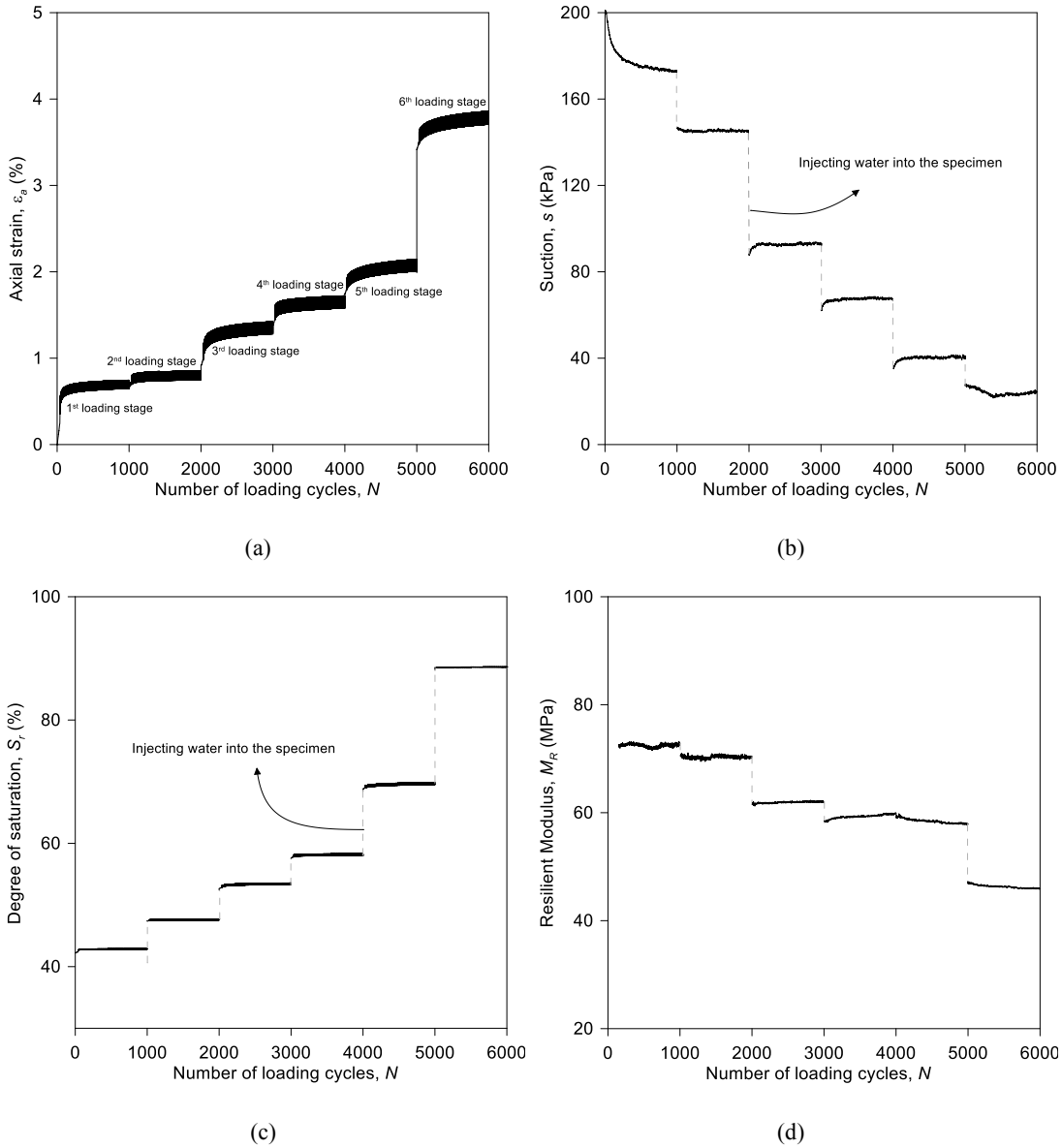

315 Fig. 6. Cyclic behaviour of 1D2q80 repetitively subjected to cyclic loads and wetting: a) axial strain, ε_a b) suction,
316 s c) degree of saturation, S_r d) resilient modulus, M_R

317

318 To investigate the effect of subsequent wetting on the strain response, 1D2q80 was repetitively subjected to
319 packets of 1000 cyclic loads and wetting as shown in Figure 6. Before applying the first packet of loads, the
320 suction was 201 kPa and the degree of saturation was 42.2%. ε_p measured after applying the first packet of the
321 cyclic loads was 0.64% (Figure 6a). After each loading stage, the specimen was wetted so the degree of saturation
322 increased, leading to subsequent reductions in the suction level (Figures 6b and 6c). The volumetric strains
323 measured during each wetting were negligible (ε_a < 0.05%). ε_a increased with the application of successive

packets of cyclic loads as the suction level decreased. The rate of the increase in ε_a jumped abruptly during the last stage of cyclic loading where the suction was 26 kPa.

It should be noted that a complete resilient state was not achieved at the end of cyclic loading from the 3rd to 6th loading stage, possibly due to the successive increases in the degree of saturation and decreases in the suction of the soil. The values of the permanent strain and resilient modulus measured for 1D2q40 after the 3rd loading stage may be slightly different from the values at the resilient state, but these differences were very small and did not lead to erroneous interpretation of the result.

Figure 6d shows M_R measured for 1D2q80 was 71.5 MPa after the first packet of loading but decreased in the following loading stages due to reductions in suction. The rate of the decrease in M_R intensified where it reduced from 58.4 MPa to 46.1 MPa during the last cyclic loading.

The results showed that the progressive saturation of the tested soil can aggravate the soil cyclic response, leading to a higher accumulation of permanent strains and lower resilient modulus under cyclic loading as the soil approaches a full saturation level.

DISSCUSSIONS AND DEVELOPING PREDICTIVE FORMULATIONS

As discussed earlier, the experimental results showed that both suction and degree of saturation are required to describe the coupled water retention and cyclic response of the tested soil. In the following, a hysteretic water retention model is formulated to simulate the water retention behaviour and predict the suction variations during cyclic loading. The implication of using Bishop′s stress and suction bonding to interpret the soil cyclic response is then discussed. Semi-empirical formulations are developed incorporating Bishop′s stress and suction bonding to predict the accumulated permanent strains and resilient modulus.

It has to be pointed out that density affects the soil water retention and cyclic behaviour. In this study, such an effect was not as significant as the effect of suction and degree of saturation as the specimens were compacted at the same density and the changes in their density were small under drying and wetting and during cyclic loading. The water retention and cyclic behaviour of the tested soil were dominantly governed by the effect of suction and degree of saturation of the specimens that were considerably different due to the applied drying and wetting paths (in addition to the effect of the cyclic deviatoric stress), so these aspects were focussed on in this study.

354 *Water retention behaviour*

355 First, a model was formulated to capture the soil water retention behaviour discussed in Figure 2a. The main
356 WRCs were simulated using the model proposed by van Genuchten (1980). For drying $S_r = S_d$:

357

$$S_d = \frac{1}{(1 + \alpha_d {s_d}^{n_d})^{1-\frac{1}{n_d}}} \qquad \Delta S_r < 0 \qquad (4a)$$

and for wetting $S_r = S_w$:

$$S_w = \frac{1}{(1 + \alpha_w {s_w}^{n_w})^{1-\frac{1}{n_w}}} \qquad \Delta S_r > 0 \qquad (4b)$$

358

359 where S_d is the degree of saturation on the main drying curve and α_d and n_d are the corresponding drying
360 parameters, and S_w is the degree of saturation on the main wetting curve and α_w and n_w are the corresponding
361 wetting parameters. α_d is calibrated based on the inverse of the air entry value of the drying water retention curve
362 and α_w is based on the inverse of the air occlusion value of the main wetting water retention curve. As the air
363 entry value is expected to be greater than the air occlusion value, always $\alpha_d < \alpha_w$. n_d and n_w are also calibrated
364 using the main drying and wetting curves obtained from water retention tests, respectively. Unreasonable values
365 must not be assumed (e.g. $n_d >> n_w$) as it may lead to the incorrect prediction of a wetting water retention curve
366 that lies above a drying water retention curve ($S_w > S_d$ at a given suction).
367 s_d and s_w are the suction values on the main drying and wetting curves, respectively. The scanning curves were
368 simulated employing incremental formulations for $S_w < S_r < S_d$:

369

$$\Delta S_r = -k \frac{(1+s)}{s_d} \frac{\Delta s}{s} \qquad \Delta S_r < 0 \qquad (5a)$$

$$\Delta S_r = -k \frac{s_w}{(1+s)} \frac{\Delta s}{s} \qquad \Delta S_r > 0 \qquad (5b)$$

370

371 where k controls the shape of the scanning curves and needs to be calibrated in a way that it avoids any divergency
372 between scanning and main curves and allows transitions between the scanning and main domains. Although a
373 simple form of this formula, i.e. $k\frac{\Delta s}{s}$, can also predict a similar line in the scanning domain, it was found not to

completely simulate the shape of the continuous experimental water retention data shown in Figure 2a. Therefore, the additional terms, $\frac{(1+s)}{s_d}$ for drying and $\frac{s_w}{(1+s)}$ for wetting, were added to consider the ratio between the current suction (s) and the suction on the main curves (s_d or s_w) which allowed better prediction of the continuous experimental water retention data. Table 3 provides values of the parameters used to simulate the observed hysteretic water retention behaviour. Figure 7 shows the model captured the experimental scanning and main WRCs well.

Table 3. Parameters of the water retention model

Hydraulic path	Model parameter		
Drying	α_d	n_d	k
	0.031	1.33	0.14
Wetting	α_w	n_w	
	0.27	1.28	

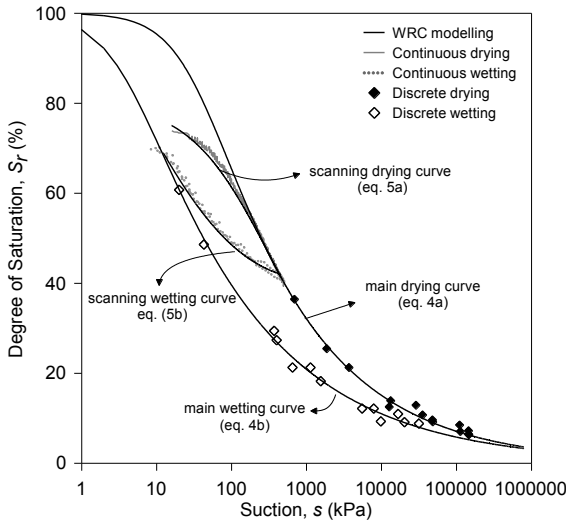

Fig. 7. Water retention behaviour of the tested soil and model prediction

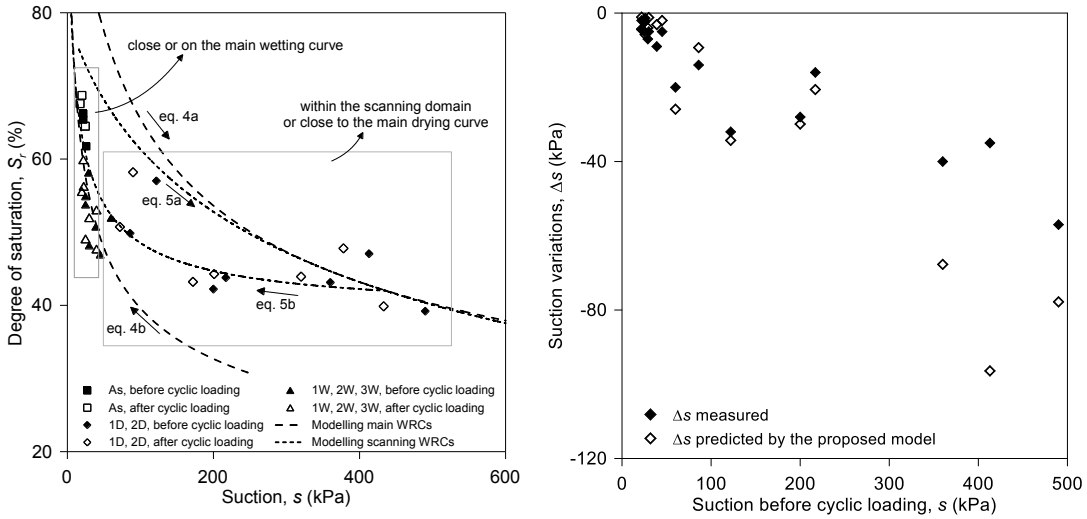

(a) (b)

Fig. 8. a) water retention behaviour of the specimens subjected to cyclic loading b) predicted and measured suction variations during cyclic loading

Figure 8a shows the predicted scanning and main WRCs and the suction values of the specimens measured before and after applying cyclic loads. The suction of the dried specimens (1D and 2D) was within the scanning domain or close to the main drying curve where the decreases in suction during cyclic loading were evident as the suction shifted towards the main wetting curve even with a small increase in the degree of saturation. The suction of the as-compacted (As) and wetted (1W, 2W and 3W) specimens was close to the main wetting curve. The water retention behaviour of these specimens during cyclic loading evolved along the main wetting curve where the increase in the degree of saturation was evident. However, the decrease in the suction level of these specimens was less pronounced than that of the dried specimens.

Next, the proposed water retention model was used to predict suction variations Δs during cyclic loading where ΔS_r of the specimens was obtained from the measured volumetric strains and constant water content. Since the degree of saturation increased, the equations proposed for the wetting path were used: equation 4b in the case of $S_r = S_w$ (corresponds to the main wetting curve) and equation 5b in the case of $S_r > S_w$ (corresponds to the scanning curves). The two equations were rearranged to obtain the suction variations Δs:

$$\Delta s = -\frac{s^{n_w-1}\Delta S_r}{\alpha_w n_w (n_w-1)}\left(1+\alpha_w s^{n_w}\right)^{2-\frac{1}{n_w}} \qquad S_r = S_w \qquad (6)$$

and

$$\Delta s = -\frac{s(1+s)\Delta S_r}{s_w k} \qquad S_r > S_w \qquad (7)$$

Equations 6 and 7 imply that the change in suction Δs is dependent on both the suction level and changes in the degree of saturation ΔS_r where Δs intensifies if s or ΔS_r increases. Under similar ΔS_r, Δs predicted by the scanning curve (equation 7) results in greater values compared to Δs predicted by the main wetting curve (equation 6) because the weight of suction in equation 7 is greater than its weight in equation 6. This is consistent with the greater suction reductions observed at high suction levels during cyclic loading. When the water retention behaviour changed along the main wetting curve, suction was low so the effect of ΔS_r was more marked compared to high suction levels. Figure 8b shows the predicted and measured suction variations with respect to the suction values obtained before applying the cycles.

It has to be noted that the soil water retention behaviour within the scanning domain is likely be dependent on different parameters such as soil fabric, density, etc. For simplification, such effects were neglected in this study to emphasise the effect of hysteresis and transition between main and scanning water retention domains. Figure 8b shows that the model predictions for the suction level greater than 300 kPa were not as accurate as the model employs only one parameter (k) to control the shape of the predicted curves under both drying and wetting paths. Although the proposed model slightly overestimated Δs at high suctions, the predicted and measured suction variations are consistent and the predicted suction values are in good agreement with the suction values measured after applying the cyclic loads as shown in Figure 9.

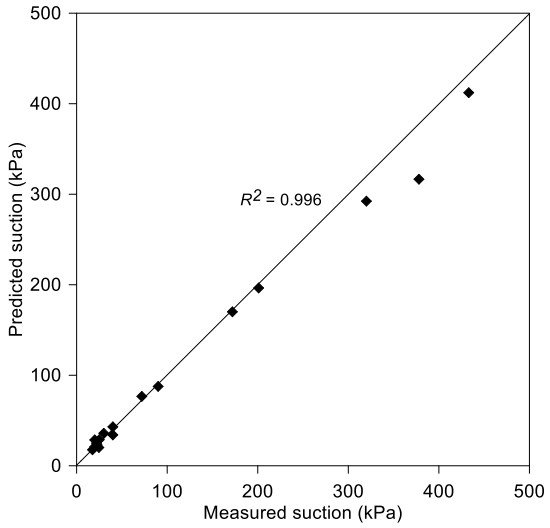

Fig. 9. Predicted and measured suction after applying cyclic loading

The proposed hysteretic water retention model allows simulating the soil water retention response and predicting suction that is required to develop predictive formulations for the soil cyclic behaviour.

Accumulated permanent deformation

Figure 10a shows the accumulated permanent strains measured for the specimens subjected to different hydraulic paths and q_{cyc} of 40 kPa in terms of mean Bishop′s stress (p^*). p^* was obtained as

$$p^* = p_n + S_r s \tag{8}$$

where p_n is the mean net stress. For the calculations, suction and degree of saturation measured at the end of cyclic loading were used as they were more relevant to the permanent strain and resilient modulus obtained at the resilient state.

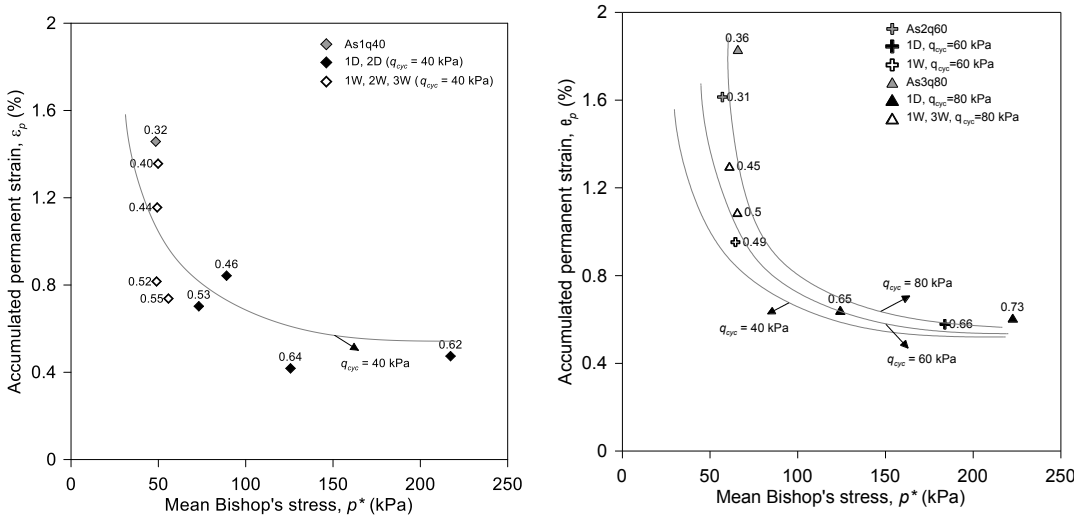

(a) (b)

Fig. 10. Accumulated permanent strains with mean Bishop′s stress and bonding parameter a) in case q_{cyc} = 40 kPa b) in cases q_{cyc} = 40, 60 and 80 kPa

As mean Bishop′s stress increased, ε_p substantially decreased. Although mean Bishop′s stress incorporated both suction and degree of saturation, it cannot exclusively capture all the measured ε_p as some data points deviated from the trendline drawn to fit the experimental data. This was more evident considering ε_p of the wetted

specimens where the measured strains changed dramatically at the same level of Bishop′s stress. This can be explained as Bishop′s stress considers the effect of suction and degree of saturation on the average soil skeleton stress whereas their effect on the normal force acting at soil particle contacts due to water menisci is neglected. Generally, the bonding inter-particle force depends on different factors such as contact angle, surface tension, size of particles, shape of pores, etc. This bonding effect was considered in this study using the bonding parameter (equation 2) formulated in terms of degree of saturation and suction only as these variables are often accessible in laboratory testing of unsaturated soils. Later in the paper, semi-empirical equations are proposed to relate the bonding parameter to the cyclic behaviour of the tested soil where phenomenological parameters are used to account for the above-mentioned factors.

Gallipoli et al. (2003) suggested values for f_s based on an inter-granular force estimated by Fisher (1926) assuming a soil consists of identical sphere particles having radii of 1 μm. $f_s = 0.838s^{0.06}$ was found to fit the values suggested by Gallipoli et al. (2003) well; hence, $\xi = (1 - S_r)0.838s^{0.06}$ was used in the present study to obtain the bonding parameter. The obtained values of the bonding parameter ξ are shown as labels of the experimental data in Figure 10a. It is worthwhile pointing out that the effects of suction on the average skeleton stress and suction bonding are regulated by the soil saturation level in different senses; the increase in the degree of saturation expands the relative area over which the water and air pressures act on the average stress but reduces the number of water menisci acting on the normal inter-particle force. At the same range of mean Bishop′s stress, ε_p of those specimens with a lower bonding parameter was higher and above the trendline ($\xi < 0.5$) whereas the specimens having higher bonding parameters ($\xi > 0.5$) exhibited lower permanent deformations and their measured ε_p lay below the trendline.

Figure 10b shows the accumulated permanent strains measured for all specimens which decreased sharply as p^* increased while approaching a steady level at higher stresses. ε_p enlarged as q_{cyc} increased from 40 kPa to 60 kPa and 80 kPa but this increase became less evident with the increase in p^*. For the specimens having $p^* \approx 40$ kPa and being subjected to q_{cyc} of 80 kPa, the effect of the suction bonding was also visible where ε_p decreased as the bonding parameter increased from 0.36 (as-compacted) to 0.45 (3rd wetting) and 0.50 (1st wetting). ε_p measured showed that the increase in q_{cyc} and the decrease in the bonding parameter resulted in an increase in the permanent deformation but such effects diminished as mean Bishop′s stress or suction bonding increased. Both Bishop′s stress and suction bonding provided stabilising effects that reduced the effect of q_{cyc} on the measured strains.

The results discussed above showed that the number of the applied hydraulic cycles induced no significant effect on the measured strains. However, changes in the soil water retention properties due to the different hydraulic

history and hysteretic water retention behaviour along the drying and wetting paths were found to significantly affect the accumulated permanent deformations and result in different strains from those measured for the as-compacted soil. Different values of suction and degree of saturation altered both mean Bishop′s stress and suction bonding acting on the specimens. An increase in suction stress $S_r s$ modified the average soil skeleton stress and minimised the possibility of slippage at the particle contacts; therefore, it reduced the accumulation of permanent strains induced by cyclic loading. The possibility of such slippages was also influenced by the stabilising effect of the normal force exerted at the soil inter-particle contacts by water menisci. The meniscus lenses of water within the tested soil under unsaturated states made the inter-particle contacts more stable, and therefore restrained the reciprocal slippage of soil particles that causes permanent deformation under cyclic loading. The bonding parameter ξ can incorporate the latter stabilising effect where ε_p decreased with an increase in the bonding parameter as well as Bishop′s stress. It has to be noted that the wetted specimens had similar suction values but different degrees of saturation where suction bonding decreased with the increase in the degree of saturation leading to the greater accumulation of strains.

In order to develop a formulation for predicting the accumulated permanent strains, Bishop′s stress ratio η^* was introduced:

$$\eta^* = \frac{q_{max}}{p^*} \tag{9}$$

where q_{max} is q_{cyc} plus the resting stress (10 kPa).

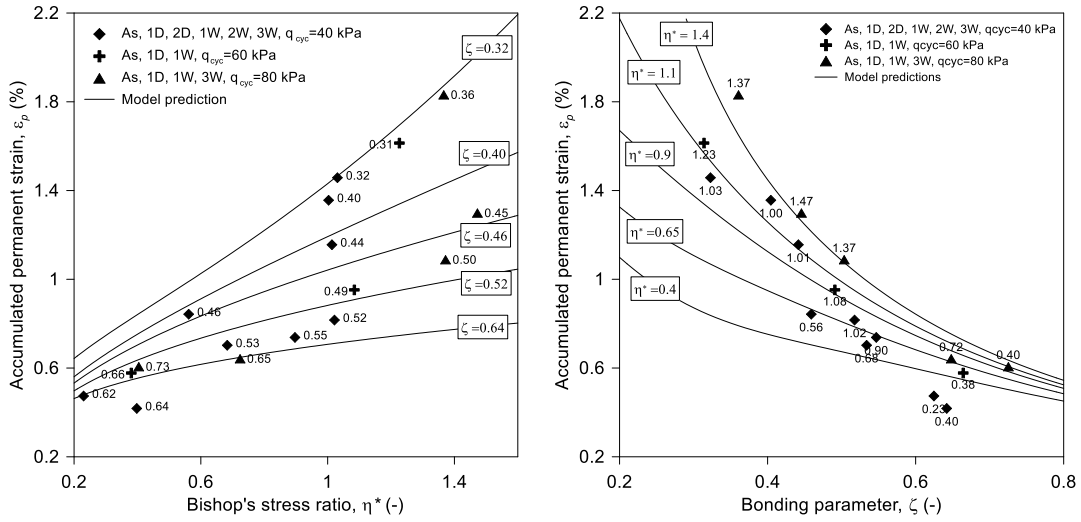

(a) (b)

491 Fig. 11. Experimental data and predictions of accumulated permanent strains a) in terms of Bishop′s stress ratio
492 b) in terms of bonding parameter
493
494 Figure 11a shows the measured ε_p in terms of Bishop′s stress ratio where the labels are the values of the bonding
495 parameters. ε_p increased with Bishop′s stress ratio and decreased with the bonding parameter. A new semi-
496 empirical formulation was then developed incorporating the effects of Bishop′s stress ratio and suction bonding
497 to predict the accumulated permanent strain:
498

$$\varepsilon_p = \eta^{*f_\xi}\left[f'_\xi\,(1 + m_1\, f'^{(m_2-1)}_\xi\, \eta^{*(\alpha - f_\xi)})\right] \tag{10}$$

499
500 where

$$f_\xi = n_1 \exp(-n_2 \xi) \tag{11}$$

501 and

$$f'_\xi = \frac{1}{1+\exp(\xi)} \tag{12}$$

502 n_1, n_2, m_1, m_2 and α are model parameters.
503 The first term incorporates Bishop′s stress ratio where η^{*f_ξ} defines the permanent strain in terms of the stress
504 ratio and f_ξ allows controlling the rate of the change in ε_p with the bonding parameter regulated by n_1 and n_2. The
505 rate of increase in the permanent strain predicted by the model reduces with the increase in the bonding parameter

as the soil becomes more stable with the increase in the inter-granular bonding forces. The second term directly accounts for the effect of the inter-granular bonding force. f_{ξ}' incorporates the effect of the bonding parameter and allows shifting the level of the predicted permanent strain with changes in the bonding parameter using $m_1$and m_2. The obtained experimental data showed that the permanent strains measured at low stress ratios converge toward a constant value regardless of the bonding parameter. Bishop's stress ratio is also introduced in the second term where α controls the predicted values at low stress ratios. The parameters are calibrated based on the best-fit using the regression method for data points represented in terms of the $\varepsilon_p - \eta^*$ graph. The parameters obtained for the tested soil are presented in Table 4.

Table 4. Parameters of the models proposed to predict the cyclic behaviour of the tested soil

Model parameters for predicting ε_p	n_1	n_2	m_1	m_2	α
	19.7	7.3	91.2	5.2	0.3
Model parameters for predicting M_r	k_1	k_2	k_3	M_0	
	2.57	2.52	0.73	46	

The accumulated permanent strains predicted by equation 10 under constant values of the bonding parameter are shown in Figure 11a. The predicted curves explicitly showed that ε_p increases with η^* and decreases with ξ. The model predictions show that the specimens having lower bonding parameters (ξ < 0.46) exhibited high accumulated permanent strains where the rate of the increase in ε_p became greater with η^*. ε_p of the specimens having higher bonding parameters (ξ > 0.46) were smaller and increased with η^* gently. When the bonding parameter was low, the slippage of soil particles was facilitated and the soil became more prone to larger accumulations of strains with the increase in η^* (i.e. increase in q_{cyc} or decrease in p^*). When the bonding parameter increased, suction bonding improved the stabilising effect and restrained the effect of η^* on the measured ε_p.

Figure 11b shows ε_p in terms of the bonding parameter (the labels are η^*). The values of ε_p measured at different stress ratios reduced as the bonding parameter increased. The contours predicted by equation 10 under constant values of η^* are also shown in Figure 11b where all the curves tend to merge as the bonding parameter increased. This implies that the effect of the stress level at high values of the bonding parameter was less evident. On the other hand, the model predictions show the effect of the bonding parameter was less evident where η^* = 0.4

implying that the soil cyclic response is mainly governed by the skeleton stress rather than suction bonding where Bishop′s stress is sufficiently high compared to the applied cyclic loads. The predicted values of ε_p are in good agreement with the measured values as shown in Figure 12.

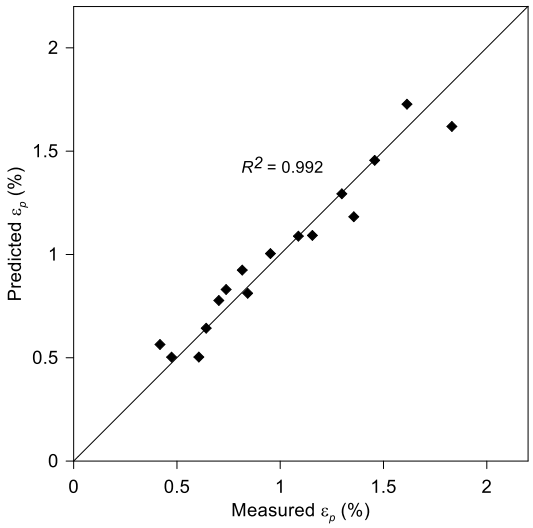

Fig. 12. Predicted and measured accumulated permanent strains

Resilient modulus

Figure 13a shows the resilient modulus M_R obtained for the tested soil with respect to mean Bishop′s stress. M_R increased with p^*. At a Bishop′s stress level about 50 kPa, M_R dramatically increased but the rate of this increase declined as the stress level exceeded 50 kPa. This deviation was also discussed by Han & Vanapalli (2016) where the resilient modulus-suction relationship was divided into two regions using the air-entry value of the soil water retention curve. M_R was also found to decrease with q_{cyc} as also reported by Yang et al. (2008) and Ng et al. (2013). Mean Bishop′s stress enlarged the effect of q_{cyc} on the resilient modulus at p^* > 140 kPa where M_R substantially decreased with q_{cyc} increasing from 40 kPa to 60 and 80 kPa. The effect of q_{cyc} on M_R may be explained by the strain level at which the permanent strain of the specimens increased with q_{cyc}; hence, the specimens exhibiting higher strains became less resilient and showed lower M_R.

The effect of suction bonding on M_R was not obvious over the whole range of mean Bishop′s stress shown in Figure 13a due to the substantial increase in the resilient modulus with an increase in p^*. Figure 13b shows the resilient modulus for $p^* \leq 140$ kPa where the data points are labelled with the values of the bonding parameter. For the specimens subjected to q_{cyc} of 40 kPa, M_R increased from 58.2 MPa to 94.5 MPa as p^* increased from 50 kPa to 126 kPa. The effect of suction bonding can be then observed comparing M_R measured for the specimens

having p^* of about 50 kPa where the increase in ξ from 0.32 to 0.55 improved the cyclic resilience of the tested soil and M_R increased from 64.9 MPa to 74.6 MPa. The increase in M_R with the bonding parameter can also be observed for the specimens subjected to q_{cyc} of 80 kPa and having p^* of about 65 kPa. The beneficial effects of ξ on M_R arise due to the fact that an increase in suction bonding induces a larger normal inter-particle force, thereby enhancing the cyclic resilience of the tested soil.

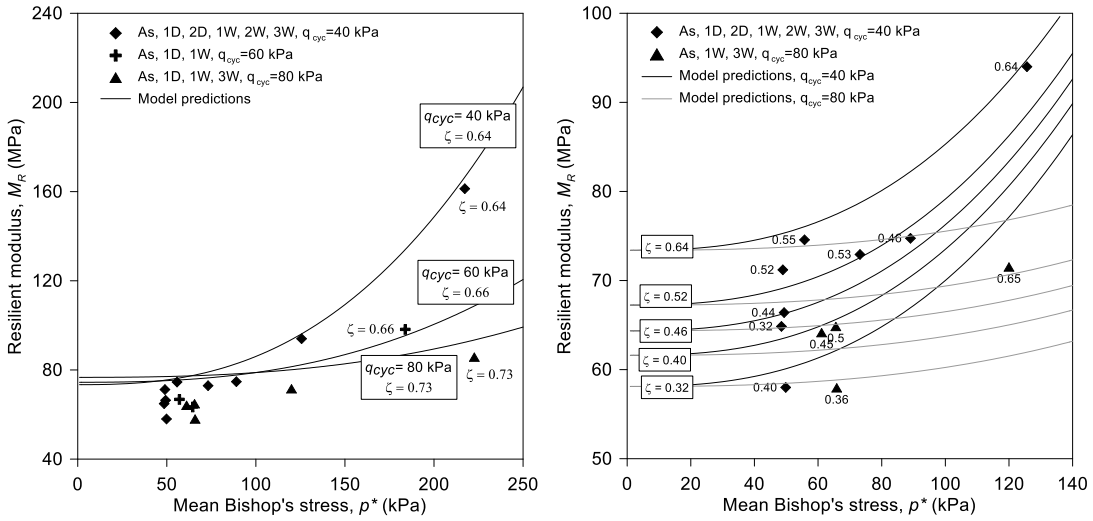

(a) (b)

Fig. 13. Experimental data and predictions of resilient modulus a) in terms of mean Bishop′s stress b) in case p^* ≤ 140)

It has to be pointed out that mean Bishop′s stress and cyclic deviatoric stress affect the resilient modulus of the tested soil predominantly whereas the effect of the bonding parameter on the resilient modulus was found to be more evident at lower stress levels. This can be partly due to the fact that M_R is greatly affected by a combined effect of the stress and strain levels. It may also be related to the hydraulic history of the tested specimens. The wetted specimens had lower values of mean Bishop′s stress as they were wetted to a limited suction range of 20 - 40 kPa. The water adsorption rate along the main wetting path abruptly changed, leading to different saturation levels and in turn varied suction bonding. On the other hand, the dried specimens had very different suction levels where the difference in Bishop′s stress was more pronounced. This indicates that the influence of suction bonding on M_R was more evident on the wetted specimens whereas the resilience of the dried specimens was dominantly influenced by the stress level.

A semi-empirical equation was then developed to predict M_R:

$$M_R = (p^*/p_r)^{k_1}.\left(1 + q_{cyc}/p_r\right)^{-k_2} + M_0\exp(k_3\xi) \quad (13)$$

where p_r = 1 is the reference mean stress (in kPa). k_1, k_2, M_0 and k_3 are model parameters. The proposed formulation takes a form similar to the one proposed by Gupta et al. (2007), but incorporating Bishop′s stress and the bonding parameter. The first term accounts for the effect of mean Bishop′s stress whereas the second term incorporates the effect of the cyclic deviatoric stress. The last term is dependent on the bonding parameter and allows independent consideration of the contribution of the bonding parameter to the resilient modulus. k_1, k_2 are calibrated based on the effect of p^* and q_{cyc} on the resilient modulus, respectively. M_0 is the reference resilient modulus in the saturated state and k_3 is calibrated considering the effect of ξ on M_R. The parameters obtained for the tested soil are presented in Table 4.

Figures 13a and 13b show the predictions of the proposed model while the predicted curves correspond to the values of M_R at constant values of ξ. The proposed model was able to capture the M_R values obtained at high mean stresses and also the reductions in M_R observed with q_{cyc} as shown in Figure 13a. Figure 13b shows that the increase in the resilient modulus with suction bonding was also predicted well at low stress levels. Figure 14 shows the experimental resilient modulus against the values predicted by equation 13 where the regression line displays a good agreement between the measured and predicted data.

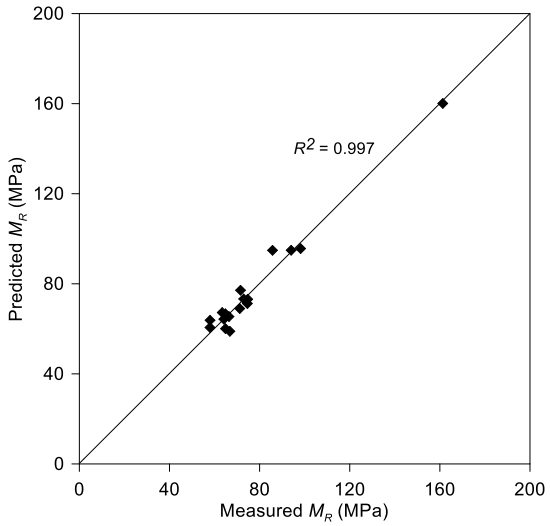

Fig. 14. Predicted and measured resilient modulus

591

592 PREDICTING SOIL RESPONSE TO REPETITIVE CYCLIC LOADING AND WETTING

593 The proposed formulations were used to predict the suction, permanent strains and resilient modulus for 1D2q80
594 that was repetitively subjected to packets of cyclic loads and wetting. Similar parameters shown in Tables 3 and
595 4 were used to predict the soil response.

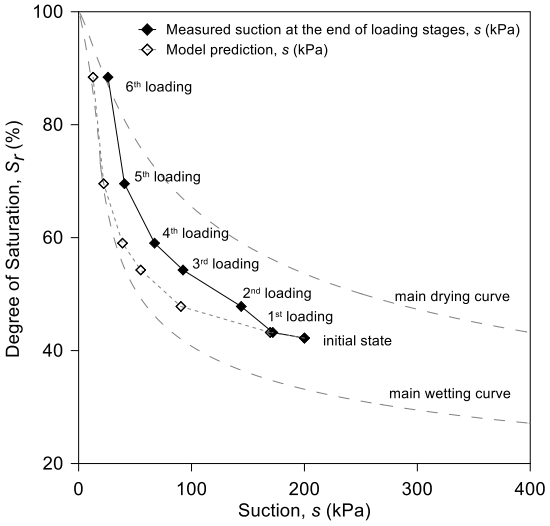

596

597 Fig. 15. Measured and predicted suction values of 1D2q80 subjected to repetitive cyclic loading and wetting

598

599 Figure 15 shows main WRCs of the tested soil and the water retention properties of 1D2q80 where the suction
600 decreased with the loading and wetting stages due to the successive increase in the degree of saturation. The
601 predicted and measured suction values matched well. Equation 7 was used to predict the suction for the first 4
602 stages (for the scanning domain, $S_r > S_w$) and equation 6 was used to predict the suction values for the last 2 stages
603 where the degree of saturation lay on the main wetting curve ($S_r = S_w$).

604

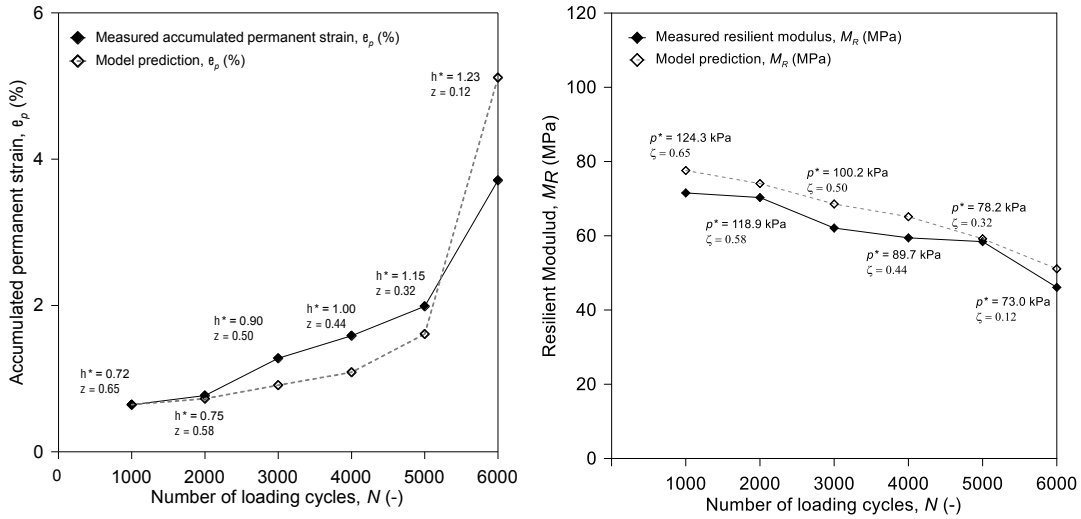

(a) (b)

Fig. 16. Experimental data and predictions of the response of 1D2q80 to repetitive cyclic loading and wetting a) accumulated permanent strains, ε_p b) resilient modulus, M_R

The predicted and measured accumulated permanent strains are shown in Figure 16a. ε_p predicted was in good agreement with the measured values. Bishop′s stress ratio and the bonding parameter (shown as labels) evolved due to the reduction in suction and increase in the degree of saturation upon the loading and wetting stages. ε_p increased with the successive stages, as also predicted by the model, owing to the increase in Bishop′s stress ratio and decrease in suction bonding. The suction at the end of the last wetting stage was 26 kPa and the degree of saturation was 88.4 where ε_p substantially increased. This was also predicted by the proposed model accounting for a low value of $\xi = 0.12$ and a high value of $\eta^* = 1.23$.

The model also predicted the resilient modulus well as shown in Figure 16b. The predicted M_R decreased with the loading and wetting stages as Bishop′s stress and suction bonding decreased. The rate of the decrease in the predicted M_R intensified along the loading stages as the decrease in the bonding parameter was pronounced with the successive stages.

The accurate predictions of the water retention and cyclic response of the specimen to repetitive cyclic loading and wetting show the capability of the proposed framework in reproducing the effects of alternative field conditions, in this case periodic rainfalls followed by frequent movements of traffic, on the coupled water retention and cyclic response of the tested soil.

Most design guidelines for roads and railways (e.g. AASHTO, 1993; UIC, 1994; Network Rail, 2003) typically neglect the unsaturated state of formation layers assuming that the subgrade material is compacted in the field at optimum water content. However, water content varies with time due to the effect of changing environmental conditions such as rainfall and evaporation. As shown in the present study, such variations together with traffic-induced loads can modify the long-term behaviour (both accumulative permanent strains and resilient modulus) of the construction materials and under unfavourable conditions may lead to poor performance of substructure. Some guidelines do suggest accounting for the effect of soil moisture variation considering the effect of soil water content or saturation level (e.g. Witczak et al., 2003; ARA, 2004), but this was found not to be sufficient to predict the coupled hydro-mechanical behaviour of the formation material tested in this study. The approach proposed hereby uses Bishop′s stress and the bonding parameter and allows appropriate incorporation of the effect of the hydraulic history on the soil behaviour. The outcome showed that a predictive framework incorporating these two constitutive variables can potentially predict the long-term performance of formation materials and prevent unfavourable scenarios under cyclic traffic-induced and environmental loads, thereby mitigating the climate-risk when used at the design stage of road and railway provision.

It has to be pointed out the proposed semi-empirical equations are example models that showed how Bishop′s stress and the bonding parameter can be formulated to provide a good prediction of the accumulated permanent strain and resilient modulus of the tested soil. A wide-ranging validation is required to generalise these equations for a wider range of soil types.

CONCLUSIONS

The present study investigated the influence of the hydraulic history on the cyclic behaviour of a formation material of a railway line, in this case a compacted clayey sand. The results of cyclic triaxial tests showed that the cyclic response of the soil obtained after applying drying and wetting paths was different to that obtained immediately after compaction. This implies that seasonal variations affect the long-term performance of the railway formation layers under traffic loads as compacted formation materials continuously undergo drying and wetting.

Changes in soil water retention properties (suction and degree of saturation) along the drying and wetting paths were found to significantly affect the suction variations, accumulated permanent strain and resilient modulus during cyclic loading. The measured accumulated permanent strain and resilient modulus were described using two constitutive variables: Bishop′s stress and suction bonding. This allowed incorporating the effect of the

hydraulic history on the cyclic response of the tested soil as both constitutive variables evolve with changes in suction and degree of saturation. The experimental results showed that:

- The measured suction decreased during cyclic loading due to the increase in the degree of saturation. The decrease in suction was more evident for the specimens being dried compared to the as-compacted and wetted specimens. This was explained by the hysteretic nature of the soil water retention behaviour.
- The accumulated permanent strains reduced with an increase in Bishop′s stress and suction bonding as the increase in soil skeleton stress and inter-particle bonding force provided the stabilising effects and inhibited slippage at particle contacts. The increase in the cyclic deviatoric stress resulted in an increase in the permanent deformation but such effect diminished as mean Bishop′s stress and suction bonding increased.
- The resilient modulus was found to increase with Bishop′s stress and decreased with the cyclic deviatoric stress. It also increased with suction bonding which was more evident at lower stress levels where the wetted specimens had pronounced varied suction bonding.
- For the test where the specimen was repeatedly subjected to cyclic loading and wetting, the progressive saturation and reductions in Bishop′s stress and suction bonding led to subsequent increases in the permanent strains and decreases in the resilient modulus.

A predictive framework was then proposed using (i) a hysteretic water retention model to predict water retention behaviour and suction variations during cyclic loading and (ii) semi-empirical formulations incorporating Bishop′s stress and the bonding parameter to predict the accumulated permanent strain and resilient modulus. The predicted and experimental data were in good agreement showing that the proposed approach was able to account for the effects of the hydraulic history on the coupled water retention and cyclic behaviour of the tested soil. This allows considering the coupled effect of cyclic traffic-induced and environmental loads on the long-term performance of unsaturated formation materials and developing strategies to mitigate the climate-risks for the design of road and railway embankments, leading to more sustainable construction of transportation infrastructure.

683 ACKNOWLEDGEMENT

684 The authors would like to acknowledge the funding received from UK Engineering and Physical Research Council
685 (EPSRC) through Global Challenges Research Fund (GCRF) to carry out the research titled 'Sustainability and
686 resilience of transportation infrastructure in African countries' grant number- EP/P029671/1. The authors would
687 like to thank the logistical support by University of Pretoria (South Africa), particularly Professor P.J. (Hannes)
688 Gräbe and Dr Sydney Laryea.

689 REFERENCES

690 AASHTO. (1993). AASHTO guide for design of pavement structures, 4th edn. Washington, DC, USA: American
691 Association of State Highway and Transportation Officials.

692 ARA, Inc., ERES Consultants Division. (2004). Guide for mechanistic–empirical design of new and rehabilitated
693 pavement structures. Final Rep., NCHRP Project 1-37A, Transportation Research Board, Washington, DC.

694 Bishop, A. W. (1959). The principle of effective stress. Tecknisk Ukeblad 106, No. 39, 859–863.

695 Blackmore, L., Clayton, C. R. I., Powrie, W. Priest, J. A. & Otter, L. (2020). Saturation and its effect on the
696 resilient modulus of a pavement formation material. *Géotechnique*, 70 (4), 292-302.

697 British Standards Institution (1990) BS 1377: Part 2: Classification tests. BSI, Milton Keynes.

698 British Standards Institution (1990) BS 1377: Part 4: Compaction-related tests. BSI, Milton Keynes.

699 Brown, S. F. (1996). Soil mechanics in pavement engineering. *Géotechnique*, 46(3): 383–426.

700 Cao, Z., Chen, J., Cai, Y., Gu, C. & Wang, J. (2017). Effects of moisture content on the cyclic behavior of crushed
701 tuff aggregates by large-scale triaxial test. *Soil Dynamics Earthquake Engineering*, 95:1–8.

702 Chen, J., Alonso, E. E., Gu, C., Cao, Z. & Cai, Y. (2018). Long term cyclic behavior of unsaturated granular soils,
703 *Transportation Geotechnics*, 17, 48-55.

704 Craciun, O. & Lo, S. (2010). Matric Suction Measurement in Stress Path Cyclic Triaxial Testing of Unbound
705 Granular Base Materials. *Geotechnical Testing Journal*, 33(1), 33-44.

706 Drumm, E. C., Reeves, J. S., Madgett, M. R., & Trolinger,W. D. (1997). Subgrade resilient modulus correction
707 for saturation effects. *Journal of Geotechnical and Geoenvironmental Engineering*, 123(7): 663–670.

708 Fisher, R. A. (1926). On the capillary forces in an ideal soil; correction of formulae given by W.B. Haines. *Journal*
709 *of Agricultural Science*, 16(3): 492-505.

710 Fredlund, D. G., Bergan, A.T. & Wong, P. K., (1977(. Relationship between modulus and stress conditions for
711 cohesive subgrade soils. *Transp. Res. Rec.*, 642, 71–81.

712 Fredlund, D. G., & Morgenstern, N. R. (1977). Stress state variables for unsaturated soils. *J. Geotech. Eng.* Div.,
713 Am. Soc. Civ. Eng., 103(5), 447–466.

714 Gallipoli, D., Gens, A., Sharma, R. & Vaunat, J. (2003). An elasto-plastic model for unsaturated soil incorporating
715 the effects of suction and degree of saturation on mechanical behaviour. *Géotechnique*, 53(1):123–135.

716 Gräbe, P. J. & Clayton, C. R. I. (2009). Effects of Principal Stress Rotation on Permanent Deformation in Rail
717 Track Foundations, *Journal of Geotechnical and Geoenvironmental Engineering*, 135(4): 555-565.

718 Gupta, S. C., Ranaivoson, A., Edil, T. B., Benson, C. H. & Sawangsuriya, A. (2007). Pavement design using
719 unsaturated soil technology, Minnesota Dept. of Transportation, St. Paul, MN.

720 Han, Z., & Vanapalli, S. K. (2015). Model for predicting the resilient modulus of unsaturated subgrade soil using
721 the soil-water characteristic curve. *Canadian Geotechnical Journal*, 52(10), 1605–1619.

722 Han, Z. & Vanapalli, S. K. (2016). State-of-the-art: prediction of resilient modulus of unsaturated subgrade soils.
723 *International Journal of Geomechanics*, 16(4):04015104.

724 Heath, A. C., Pestana, J. M., Harvey, J. T. & Bejerano, M. O. (2004). Normalizing behavior of unsaturated
725 granular pavement materials. *Journal of Geotechnical and Geoenvironmental Engineering*, 9, 896–904.

726 Hu, R., Liu, H. H., Chen, Y. F., Zhou, C. B. & Gallipoli, D. (2014). A Constitutive Model for Unsaturated Soils
727 with Consideration of Inter-particle Bonding. *Computers and Geotechnics*, 59, 127–144.

728 Jommi, C. (2000). Remarks on the constitutive modelling of unsaturated soils. In Experimental evidence and
729 theoretical approaches in unsaturated soils (eds A. Tarantino and C. Mancuso), pp. 139–153. Rotterdam, the
730 Netherlands: Balkema (Taylor & Francis Group).

731 Khalili, N, Habte, M. A. & Zargarbashi, S. (2008). A fully coupled flow deformation model for cyclic analysis of
732 unsaturated soils including hydraulic and mechanical hysteresis. *Computers and Geotechnics*, (6): 872-889.

733 Khoury, C. N., Khoury, N.N. & Miller, G. (2011). Effect of cyclic suction history (hydraulic hysteresis) on
734 resilient modulus of unsaturated fine-grained soil. *Transp Res Rec J Transp Res Board*, 2232:68–75

735 Khoury, N. N., Brooks, R. & Khoury, C. N. (2009). Environmental influences on the engineering behavior of
736 unsaturated undisturbed subgrade soils: Effect of soil suctions on resilient modulus. *International Journal of*
737 *Geotechnical Engineering*, 3(2), 303–311.

738 Kumar, A., Azizi, A. & Toll, D. G. (2021). On the application of suction monitoring technique for cyclic triaxial
739 testing for compacted subgrade soil. Submitted to *Journal of Geotechnical and Geoenvironmental*
740 *Engineering*.

741 Lekarp, F., Isacsson, U. & Dawson, A. (2000). State of the art. I: Resilient response of unbound aggregates.
742 *Journal of Transportation Engineering*, 126(1): 66–75.

743 Li, D. & Selig, E. T. (1998). Method for railroad track foundation design. I: development. *Journal of Geotechnical*
744 *and Geoenvironmental Engineering*, 124(4), 316–322.

745 Liang, R. Y., Rabab'ah, S. & Khasawneh, M. (2008). Predicting moisture-dependent resilient modulus of cohesive
746 soils using soil suction concept. *Journal of Transportation Engineering*, 1(34), 34–40.

747 Liu, J. & Xio, J. (2010). Experimental Study on the Stability of Railroad Silt Subgrade with Increasing Train
748 Speed. *Journal of Geotechnical and Geoenvironmental Engineering*, 136(6): 833-841.

749 Lourenço, S. D. N., Gallipoli, D., Toll, D. G., Augarde, C., Evans, F. & Medero, G. M. (2008). Calibration of a
750 high-suction tensiometer. *Géotechnique* 58, No. 8, 659–668.

751 McCartney, J. S. & Khosravi, A. (2013). Field Monitoring System for Suction and Temperature Profiles under
752 Pavements. *Journal of Performance of Constructed Facilities*, 27(6), 818-825.

753 Network Rail. (2003). Formation treatments RT/CE/C/039. Company Code of Practice. Network Rail, 40 Melton
754 Street, London W1 2EE.

755 Ng, C. W. W., Sadeghi, H., Hossen, S. K. B., Chiu, C. F., Alonso, E. E. & Baghbanrezvan, S. (2016). Water
756 retention and volumetric characteristics of intact and re-compacted loess. *Canadian Geotechnical Journal*,
757 53(8): 1258-1269.

758 Ng, C. W. W. & Zhou, C. (2014). Cyclic behaviour of an unsaturated silt at various suctions and temperatures.
759 *Géotechnique*, 64, No. 9, 709–720.

760 Ng, C. W. W., Zhou, C., Yuan, Q. & Xu, J. (2013). Resilient modulus of unsaturated subgrade soil: experimental
761 and theoretical investigations. *Canadian Geotechnical Journal*, 50(2): 223–232.

762 Oh, J. H., Fernando, E. G., Holzschuher, C. & Horhota, D. (2012). Comparison of resilient modulus values for
763 Florida flexible mechanistic-empirical pavement design. *International Journal of Pavement Engineering*,
764 13(5), 472–484.

765 Oloo, S. Y. & Fredlund, D. G. (1998). The application of unsaturated soil mechanics theory to the design of
766 pavements. Proc. 5th Int. Conf. on the Bearing Capacity of Roads and Airfields, Tapir Academic Press,
767 Trondheim, Norway, 1419–1428.

768 Romero, E., Della Vecchia, G. & Jommi, C. (2011). An insight into the water retention properties of compacted
769 clayey soils. *Géotechnique* 61(4), 313–328.

770 Salour, F. & Erlingsson, S. (2015). Resilient modulus modelling of unsaturated subgrade soils: laboratory
771 investigation of silty sand subgrade. *Road Material Pavement Design*, 16, No. 3, 553–568.

772 Seed, H. B., Chan, C. K. & Lee, C. E. (1962). Resilience characteristics of subgrade soils and their relation to
773 fatigue failures, Proceedings of the International Conference on Structural Design of Asphalt Pavements, Ann
774 Arbor, Michigan, pp. 611–636.

775 Sivakumar, V., Kodikara, J., O'Hagan, R., Hughes, D., Cairns, P. & McKinley, J. D. (2013). Effects of confining
776 pressure and water content on performance of unsaturated compacted clay under repeated loading.
777 *Géotechnique*, 63(8), 628–640.

778 Stirling, R. A., Toll, D. G., Glendinning, S., Helm, P. R., Yildiz, A., Hughes, P. N., Asquith, J. D. (2020). Weather-
779 driven deterioration processes affecting the performance of embankment slopes. *Géotechnique*, 1-27.

780 Tarantino, A. (2007). A possible critical state framework for unsaturated soils. *Géotechnique*, 57, No. 4, 385–389.

781 Tarantino, A. & Tombolato, S. (2005). Coupling of hydraulic and mechanical behaviour in unsaturated compacted
782 clay. *Géotechnique*, 55, No. 4, 307–317.

783 Thom, R., Sivakumar, V., Brown, J. & Hughes, D. (2008). A simple triaxial system for evaluating the performance
784 of unsaturated soils under repeated loading. *Geotechnical Testing Journal*, 31(2), 1–8.

785 Tripathy, S., Tadza, M. Y. M. & Thomas, H. R. (2014). Soil-water characteristic curves of clays. *Canadian*
786 *Geotechnical Journal*, 51(8): 869-883.

787 Toll, D. G. (1990). A framework for unsaturated soil behaviour. *Géotechnique*, 40, No. 1, 31–44.

788 Toll, D. G., Lourenço, S. D. N. & Mendes, J. (2013). Advances in suction measurements using high suction
789 tensiometers. *Engineering Geology*, 165, 29–37.

790 Toll, D. G. & Ong, B. H. (2003). Critical-state parameters for an unsaturated residual sandy clay. *Géotechnique*,
791 53, No. 1, 93–103.

792 UIC (1994). UIC Code 719 R. Earthworks and track-bed layers for railway lines. International Union of Railways,
793 Paris, France.

794 van Genuchten, M. T. (1980). A closed-form equation for predicting the hydraulic conductivity of unsaturated
795 soils. *Soil Science Society American Journal*, 44, No. 5, 892–898.

796 Wheeler, S. (1996). Inclusion of specific water volume within an elastoplastic model for unsaturated soils.
797 *Canadian Geotechnical Journal*, 33:42–57. 5.1

798 Wheeler, S. J., Sharma, R. S. & Buisson M. S. R. (2003). Coupling of hydraulic hysteresis and stress-strain
799 behaviour in unsaturated soils. *Géotechnique*, 53(1): 41–54

800 Witczak, M. W. (2003). NCHRP 1-28A: Harmonized test method for laboratory determination of resilient
801 modulus for flexible pavement design. Final Report. TRB, National Research Council, Washington, D.C.

802 Yang, S. R., Lin, H. D., Kung, H. S. & Huang, W. H. (2008). Suction-controlled laboratory test on resilient
803 modulus of unsaturated compacted subgrade soils. *Journal of Geotechnical and Geoenvironmental*
804 *Engineering*, 134(9):1375–1384.

805 Zhou, C. & Ng, C. W. W. (2016). Simulating the cyclic behaviour of unsaturated soil at various temperatures
806 using a bounding surface model. *Géotechnique*, 66(4): 344-350.

807
808
809
810
811
812
813
814
815
816
817
818
819
820
821
822
823
824

List of Figures

876 *List of Tables*